Biochimica et Biophysica Acta 1807 (2011) 1044–1055

Contents lists available at ScienceDirect

Biochimica et Biophysica Acta

journal homepage: www.elsevier.com/locate/bbabio

Monomeric RC–LH1 core complexes retard LH2 assembly and intracytoplasmic membrane formation in PufX-minus mutants of *Rhodobacter sphaeroides*

Peter G. Adams, David J. Mothersole, Irene W. Ng, John D. Olsen, C. Neil Hunter *

Department of Molecular Biology and Biotechnology, University of Sheffield, Sheffield S10 2TN, United Kingdom

ARTICLE INFO

Article history:
Received 7 April 2011
Received in revised form 18 May 2011
Accepted 19 May 2011
Available online 2 June 2011

Keywords:
Bacterial photosynthesis
Light-harvesting
Membrane protein
Protein assembly
PufX
Atomic force microscopy

ABSTRACT

In the model photosynthetic bacterium *Rhodobacter sphaeroides* domains of light-harvesting 2 (LH2) complexes surround and interconnect dimeric reaction centre–light-harvesting 1–PufX (RC–LH1–PufX) 'core' complexes, forming extensive networks for energy transfer and trapping. These complexes are housed in spherical intracytoplasmic membranes (ICMs), which are assembled in a stepwise process where biosynthesis of core complexes tends to dominate the early stages of membrane invagination. The kinetics of LH2 assembly were measured in PufX mutants that assemble monomeric core complexes, as a consequence of either a twelve-residue N-terminal truncation of PufX (PufXΔ12) or the complete removal of PufX (PufX$^-$). Lower rates of LH2 assembly and retarded maturation of membrane invagination were observed for the larger and less curved ICM from the PufX$^-$ mutant, consistent with the proposition that local membrane curvature, initiated by arrays of bent RC–LH1–PufX dimers, creates a favourable environment for stable assembly of LH2 complexes. Transmission electron microscopy and high-resolution atomic force microscopy were used to examine ICM morphology and membrane protein organisation in these mutants. Some partitioning of core and LH2 complexes was observed in PufX$^-$ membranes, resulting in locally ordered clusters of monomeric RC–LH1 complexes. The distribution of core and LH2 complexes in the three types of membrane examined is consistent with previous models of membrane curvature and domain formation (Frese et al., 2008), which demonstrated that a combination of crowding and asymmetries in sizes and shapes of membrane protein complexes drives membrane organisation.

1. Introduction

Light-harvesting (LH) complexes act as protein scaffolds for pigments, and form densely-packed, oriented networks for capture of light and subsequent energy transfer to the reaction centre (RC) traps [1]. In many photosynthetic bacteria peripheral light-harvesting 2 (LH2) complexes absorb light in the visible and near-infrared (NIR) regions of the spectrum and channel excitation energy energetically downhill to RC–LH1 complexes, where the energy is trapped as a photochemical charge separation [2,3]. LH1 encircles the RC to form a 'core' complex, which can be a monomeric, roughly circular structure in some bacteria but an S-shaped dimeric structure in others (for a review of core complexes see [4]).

The organisation of LH2 and RC–LH1 core complexes in the photosynthetic membranes from several bacteria has been revealed by atomic force microscopy (AFM; for reviews see [5,6]). In the model photosynthetic bacterium *Rhodobacter* (*Rba.*) *sphaeroides* RC–LH1–PufX core complexes tend to associate with one another to form short rows of 4–5 dimeric complexes, but also with a few monomers present; both types of core complex are surrounded and interconnected by LH2-rich domains [7–9], forming extensive networks for energy transfer and trapping comprising several thousand bacteriochlorophylls (BChls) [2,3,10]. These networks are housed in intracytoplasmic membranes (ICMs) which are attached to the cytoplasmic membrane, and which also exist as both budded and 'free-living' spherical vesicles in the cytoplasm [9].

The assembly of the ICM is initiated at specialised, curved regions of the cytoplasmic membrane [9,11,12], which are enriched in the BChl biosynthesis enzyme BChl synthase [13], but deficient in energy transfer from LH2 to core complexes [9,14], as well as having impaired reduction of the cytochrome bc_1 complex [15]. Assembly of energy- and electron-transfer complexes at these curved regions requires polypeptide translocation and insertion into the membrane, post-translational modifications and protein folding, all tightly coordinated

Abbreviations: AFM, atomic force microscopy; BChl(s), bacteriochlorophyll(s); B850, bacteriochlorophyll in light-harvesting 2 complex with maximal absorption at 850 nm; B875, bacteriochlorophyll in light-harvesting 1 complex with maximal absorption at 875 nm; EDTA, ethylenediamine tetraacetic acid; HEPES, N-2-hydroxyethylpiperazine-N′-2-ethanesulfonic acid; ICM, intracytoplasmic membrane; LD, linear dichroism; LH1, light-harvesting 1 complex; LH2, light-harvesting 2 complex; NIR, near-infrared; Q-PCR, quantitative real-time polymerase chain reaction; *Rba.*, *Rhodobacter*; RC, reaction centre; RC–LH1, reaction centre–light-harvesting 1 complex; *Rsp.*, *Rhodospirillum*; *Rps.*, *Rhodopseudomonas*; TEM, transmission electron microscopy; UPB, upper pigmented band; WT, wild-type; 2-D, two-dimensional; 3-D, three-dimensional; β-DDM, β-dodecylmaltoglucoside

* Corresponding author. Tel.: +44 114 222 4191; fax: +44 114 222 2711.
E-mail address: c.n.hunter@sheffield.ac.uk (C.N. Hunter).

0005-2728/$ – see front matter © 2011 Elsevier B.V. All rights reserved.
doi:10.1016/j.bbabio.2011.05.019

with the biosynthesis and attachment of cofactors. These processes are complicated and poorly understood, and although photosynthetic assembly factors have been identified in *Rba. sphaeroides* and *Rba. capsulatus* their mode of action is relatively unknown [16–22].

The growing photosynthetic membrane acquires curvature initially as a result of assembly of dimeric RC–LH1–PufX complexes, which were shown to be present at the sites of initiation of ICM formation [9]. The membrane-curving effects of the RC–LH1–PufX dimer arise because the periplasmic halves of the complexes incline towards each other in the membrane at an angle of 146° [23,24]. The basis for the dimerisation of the RC–LH1–PufX complex is the PufX polypeptide which is an integral part of the *Rba. sphaeroides* core complex [25]. PufX is essential for efficient photosynthetic growth [26–29] and is directly responsible for dimerisation of the core complex [30,31], mediated by the cytoplasmic N-terminal domain [30,32].

Niederman and co-workers studied the formation of ICM over an 18-hour time-course, and found that absorption at 875 nm, now known to arise from RC–LH1–PufX complexes, was a major feature of NIR spectra in the first two hours, and that 800 and 850 nm absorption became dominant thereafter [33]. They proposed a stepwise assembly process, where core complexes are preferentially assembled, followed by LH2, consistent with the earlier proposal of Takemoto [34]. The observation that the sites of initiation of membrane formation, termed upper pigmented band (UPB) [11], were enriched in core complexes [35] is consistent with this stepwise model. Atomic force microscopy (AFM) and transmission electron microscopy (TEM) of these sites of membrane growth not only showed that RC–LH1–PufX dimers were present, but also that these regions retained their curvature even in a purified state [9]. Thus, it is likely that curvature is initiated at these membrane sites of membrane growth by RC–LH1–PufX dimers, which create a favourable environment for the subsequent assembly of LH2 complexes. This is a preference rather than an absolute requirement for LH2 assembly, since it has been known for some time that LH2 complexes of *Rba. sphaeroides* have their own membrane-curving properties, and indeed in the absence of core complexes LH2-only mutants assemble to form spherical ICM [36,37].

The availability of mutants that assemble monomeric core complexes, as a result of a twelve-residue N-terminal truncation of PufX (PufXΔ12) or the complete removal of PufX (PufX$^-$) [32], provides an opportunity to investigate the kinetics of LH2 assembly in membranes with a greatly reduced curvature, and to examine the hypothesis that LH2 assembly is favoured when the membrane curvature has already been established. More generally, the ability to control the size, shape and curvature of a major component of a membrane, in this case the RC–LH1 core complex, allows us to examine a previous model of membrane curvature and domain formation [38], which showed how membrane organisation can result from a combination of crowding and asymmetries in sizes and shapes of membrane protein complexes. In this study, we investigate the kinetics of LH2 assembly in PufX mutants and examine downstream effects on ICM morphology and membrane protein organisation by TEM and detailed high-resolution AFM analysis. Additionally, we test theories regarding clustering and domain formation of the core complex and analyse the dimensions of the LH complexes to align our AFM data with other high resolution structural data on LH2 and core complexes.

2. Materials and methods

2.1. Strains and standard cell culture

The *Rba. sphaeroides* mutants used in this study have been described previously [32,39–41]. The strains are transconjugants of the pRKEH10 plasmid (containing *pufBALMX*) in either a *puf*-deletion (DPF2) or *puc* + *puf* double-deletion (DD13) background. Versions of the pRKEH10 plasmid contain either a wild-type copy of *pufX*, a deletion of *pufX* or a truncation of *pufX*: (i) PufX$^+$ RC$^+$ LH1$^+$ LH2$^+$, (ii) PufX$^-$ RC$^+$ LH1$^+$ LH2$^+$, (iii) PufXΔN-12 RC$^+$ LH1$^+$ LH2$^+$ and (iv) PufX$^-$ RC$^+$ LH1$^+$ LH2$^-$ are referred to hereafter as 'pseudo wild-type', PufX$^-$ LH2$^+$, PufXΔ12 LH2$^+$ and PufX$^-$ LH2$^-$, respectively.

All strains were grown in M22+ medium supplemented with the requisite antibiotics. Semi-aerobic cultures were grown in the dark, in conditions which induce maximal pigment synthesis [33], using a shaking incubator at 140 rpm at 30 °C, in conical flasks at 75% capacity.

2.2. Induction of membrane assembly in oxygen-limited cultures

Cells were grown aerobically in highly-baffled conical flasks at 12.5% capacity to suppress formation of the photosynthetic apparatus in a shaking incubator at 250 rpm at 30 °C. Cells were harvested (4,000g, 10 min) and pellets were re-suspended in sterile medium to an absorbance of 2.0 at 680 nm in a final volume of 85 ml in a 125 ml flask to promote the oxygen-limited conditions that induce assembly of ICM [33]. Cell samples were taken at regular intervals for recording absorbance spectra, which were analysed using Origin graphical software (v7.5, OriginLab Corporation). Time-lapse difference spectra were generated by subtraction of a time zero baseline (cell scatter), after normalisation for cell density at 680 nm. Spectra were smoothed for clarity (adjacent-averaging). Normalisation for LH1 (B875 at 875 nm) allowed comparison of the accumulation of LH2 (B850 at 850 nm) relative to LH1.

2.3. Quantitative real-time polymerase chain reaction

Samples from induced cultures (Section 2.2) were taken at t = 0, 1 h, 4 h and 8 h, and immediately added to two volumes of RNAprotect™ Bacteria Reagent (Qiagen GmbH, Hilden, Germany) for RNA stabilisation. Cells were harvested and pellets stored at −80 °C. Total RNA extraction was performed from 10^9 cells using the RNeasy™ Mini Kit (Qiagen) including on-column digestion of residual genomic DNA, following the manufacturer's instructions, except for cell disruption which was by lysosome treatment (10 mg/ml) for 45 min at room temperature. Reverse transcription was performed on 4 μg RNA using SuperScript™ III Reverse Transcriptase (Invitrogen) following the manufacturer's instructions, with random primers, in a total reaction volume of 20 μl. The cDNA was immediately purified using a QIAquick™ PCR Purification Kit (Qiagen), following the manufacturer's instructions.

Quantitative real-time polymerase chain reaction (Q-PCR) was performed using the SensiMix™ SYBR Kit (Bioline) with SYBR green chemistry using a Stratagene Mx3005P instrument. Assays were performed in a 25 μl final volume with 12.5 μl of 2X SensiMix™ SYBR premix, 0.5 μM primers and 100 ng cDNA template or water for the negative control. For *pucB* assays, cDNA templates were diluted 1/100 to obtain results within the confidence range of the technique. Thermal cycling conditions were as follows: 10 min at 95 °C followed by 30 cycles of 15 s at 95 °C, 30 s at 58 °C and 15 s at 72 °C. Specificity of the PCR product was confirmed by melting curve analysis. Primers with lengths of 18–22 bases and melting temperatures of 59–61 °C were designed using Primer3 software. The following primer sets were used (5′ to 3′): (i) *pucB,* TGACGATCTGAACAAAGTCTGG (forward), GAGGAAGTGCGCGATGAG (reverse); (ii) *puhA*, TTGGTGTGACTGCTTTTGGA (forward), CATGTTCTCGGTCTGGAGGT (reverse); (iii) *gyrA*, GAGTTCGTCGGTCACTTCCT (forward), GACGGCACCTACAACCTCTC (reverse). Although there are two *pucB* genes in *Rba. sphaeroides* [42], the *pucB* primer designed for these Q-PCR experiments greatly favours amplification of the *pucB1* transcript, since there are 5 mismatches in the forward primer and three in the reverse primer in relation to the *pucB2* gene which would lower the melting temperature by 14 and 12 °C, respectively. Agarose gel electrophoresis showed that each pair of primers produced a single PCR product of the expected size from genomic DNA. The primer efficiency was determined by generating calibration curves using genomic DNA template over six orders of magnitude. Calibration curves

all had R^2 values for linearity above 0.99 and primers had efficiencies above 94%. Transcript levels were calculated from the measured C_t values using these calibrations. *PucB* and *puhA* levels were normalised for their PCR product length, to allow comparison between the calibrated amounts of DNA.

Gene expression was analysed by relative quantification against the control transcript *gyrA* (DNA gyrase subunit A), previously used as an internal standard in several bacteria [43–46]. The ratio of the level of *pucB* versus *puhA* transcripts (independent of *gyrA*) was also analysed. Duplicate parallel cultures of each mutant were analysed. All assays were performed in triplicate and the standard deviation of the combined error is displayed as error bars in the graphic analysis.

2.4. Quantification UPB and ICM levels

Cultures (grown as in Section 2.1) were harvested during exponential growth at an absorbance at 680 nm of 1.5. Cells were disrupted and fractionated to separate UPB and ICM fractions by rate-zone centrifugation as previously described [9]. Photographs were taken, pigmented fractions were harvested and their relative abundance was quantified by the total absorbance units at 850 nm (e.g. 1 unit = 1 ml of 1.0 AU or 2 ml at 0.5 AU).

2.5. Preparation of ICM vesicles

Cultures (grown as in Section 2.1) were harvested at an absorbance at 680 nm of 3.0, and cells were re-suspended in 20 mM HEPES, 5 mM EDTA (pH 7.5) at approximately 10 ml buffer per 5 g cells. Cell breakage was performed by treatment with lysozyme (1 mg/ml) for 30 min at 37 °C, then supplementation with a few crystals of DNase I prior to three passages through a French pressure cell at 3,000 psi. Unbroken cells were removed by centrifugation at 32,000×*g* at 4 °C for 20 min. The cell extract was layered onto a 15/40% (w/w) sucrose discontinuous gradient and fractionated by centrifugation at 90,000×*g* at 4 °C for 12 h. The pigmented ICM band was harvested and stored at −20 °C until required.

2.6. Preparation of cell sections

Cells from a freshly growing culture were pelleted at 3000×*g* and washed twice in 50 mM HEPES (pH 7.5). Primary fixation was performed in Karnosky's fixative (2% paraformaldehyde, 2.5% glutaraldehyde, 100 mM sodium cacodylate, pH 7.5) for 3 h at 4 °C. Cells were washed three times in 100 mM sodium cacodylate, 10% w/v sucrose, at 4 °C with 30 min intervals. Secondary fixation was carried out in 2% aqueous osmium tetroxide for 1 h at room temperature. Cells were dehydrated through a graded series of ethanol washes and then washed in propylene oxide. Infiltration was performed in a 50/50 mixture of propylene oxide/Spurr resin at room temperature, for approximately 16 h. Specimens were soaked in full strength Spurr resin for 6–8 h at room temperature then embedded in fresh Spurr resin for 24 h at 60 °C. Thin sections (60–90 nm) were cut using a Reichert Ultracut E ultra microtome equipped with a diamond knife, transferred onto formvar-coated grids and stained with 3% uranyl acetate in 50% ethanol, followed by Reynold's lead citrate.

2.7. Transmission electron microscopy (TEM)

ICM samples were applied to glow-discharged carbon-coated grids and stained with 0.75% (w/v) uranyl formate. Cell sections were prepared as above. Images were recorded at 100 kV on a Philips CM100 microscope equipped with a Gatan Ultrascan 667 CCD camera at magnifications between ×5,000 and ×52,000. Images were analysed using Digital Micrograph software (Gatan).

2.8. Preparation of membrane patches

Low concentrations of β-dodecylmaltoglucoside (β-DDM) (Glycon Biochemistry, GmbH Biotechnology, Germany) were used to form membrane patches amenable to AFM imaging from ICM vesicles, in a protocol adapted from Bahatyrova and co-workers [7]. ICM were diluted in 20 mM HEPES, 5 mM EDTA (pH 7.5) to an absorbance of 0.75 at 850 nm in a total volume of 3 ml, treated with β-DDM to 0.01 or 0.02% (w/v) and layered onto a 20–45% (w/w) sucrose continuous gradient containing a matching concentration of β-DDM. Membranes were fractionated by centrifugation at 198,000×*g* at 4 °C for 9 h. The pigmented band at approximately 35% sucrose contained purified membrane patches and was harvested and stored at −80 °C until required.

2.9. Atomic force microscopy (AFM)

Membrane patches were adsorbed for 1 h onto freshly cleaved mica (Agar Scientific) in 10 mM HEPES, 150 mM potassium chloride, 25 mM magnesium chloride (pH 7.5), then exchanged into an imaging buffer of 10 mM HEPES, 100 mM potassium chloride (pH 7.5). AFM was carried out using a Multimode microscope with a Nanoscope IV controller equipped with an 'E' scanner (15×15 μm) (Bruker Nano Surfaces Business, formerly Veeco Instruments Ltd). Sharpened SiN probes (k = 0.15 N/m) (Olympus) were used in a standard tapping mode fluid cell operating at 7–9 kHz. Parameters were optimised whilst imaging, to minimise forces exerted on the sample. Images were recorded (512×512 pixels) at scan frequencies of 0.5–1.5 Hz.

Topographs were flattened and three-dimensional (3-D) representations generated using Nanoscope (v6) and Nanoscope Analysis software (v1.20). Statistical analysis of high resolution topographs was performed using Gwyddion software (open source, v2.20) by careful measurement of height profiles across individual molecules. Only clearly defined complexes were analysed to produce the most accurate analysis. For all lateral measurements the 'peak–peak' separation was measured to allow a reproducible comparison: for RC–RC separation, between the maximal protrusions of the RC-H subunit; for LH1/LH2 diameter, between the maximal protrusions of each edge of the LH1/LH2 ring (i.e. diameter corresponds to a 'middle' diameter, in between the inner and outer limits of the ring structure). All heights were measured as the maximal protrusion of the component of interest from the mica substrate.

2.10. Simulation of absorbance spectra

Simulated spectra of the membrane patches imaged by AFM were generated using Origin graphical software (v7.5, OriginLab Corporation), using the formula:

$$(\text{core spectrum}) \times \varepsilon_1 \times (\text{ratio of counted cores} / \text{LH2}) + (\text{LH2 spectrum}) \times \varepsilon_2$$

where, 'core spectrum' = absorbance spectrum of purified ICM from a monomeric core-only strain of *Rba. sphaeroides* ($PufX^-$ $LH2^-$), normalised to an absorbance at 875 nm of 1.00; 'LH2 spectrum' = absorbance spectrum of purified ICM from the LH2-only mutant of *Rba. sphaeroides* (DPF2R), normalised to an absorbance at 850 nm of 1.00; ε_1 = extinction coefficient of $PufX^-$ or PufXΔ12 core complexes (as appropriate) at 875 nm; ε_2 = extinction coefficient of the LH2 complex at 850 nm. These extinction coefficients apply to the membrane-bound form of each complex.

$$\varepsilon_1 = 4410\ \text{mM}^{-1}\text{cm}^{-1}(\text{PufX}^-\text{core complex})$$
$$\text{or } 4670\ \text{mM}^{-1}\text{cm}^{-1}(\text{PufX}\Delta 12\ \text{core complex})$$

$$\varepsilon_2 = 3720\ \text{mM}^{-1}\text{cm}^{-1}(\text{LH2 complex}).$$

Extinction coefficients were determined as follows. The starting material was ICM purified from either (i) LH2-only, (ii) core-complex-

only (PufX$^-$) or (iii) core-complex-only (PufXΔ12) mutant strains. The BChl concentration was estimated after pigment extraction in acetone:methanol:water (7:2:1) from absorbance at 770 nm using an extinction coefficient of 76 mM^{-1} cm^{-1} [47]. Extinction coefficients were then calculated by correction for the known number of BChl per LH2 complex (18 B850 from a total of 27 BChl) and the assumed numbers of BChl in PufX$^-$ and PufXΔ12 core complexes (a total of 36 and 34 BChl, respectively).

3. Results

3.1. PufX mutants have lower rates of LH2 assembly and retarded maturation of membrane invagination

The assembly and accumulation of LH2 and core complexes over time were investigated by performing growth experiments, where assembly of photosynthetic apparatus was induced in a controlled manner by transfer of aerobically growing cells to semi-aerobic growth conditions in the dark. The relative amounts of LH2 versus the core complex in a population of cells can be estimated spectroscopically by their specific BChl absorption maxima at 850 and 875 nm (B850 and B875), respectively. Spectra from a representative culture were recorded over a time-course, to assess the relative amounts of each complex, see Fig. 1.

The assembly of LH2 and RC–LH1 complexes leads to an increase in the magnitude of the characteristic overlapping B850 and B875 peaks over time in all three mutants. It is known that during maturation of the ICM, core complexes are assembled in the membrane preferentially in the early stages, and that formation of domains of LH2 complexes subsequently dominates photosystem assembly [33]. In agreement with this, we found that the ratio of LH2 to core complex, represented as the B850:B875 ratio from the spectra in Fig. 1A, starts low and increases over time (Fig. 1B). A clear difference develops in the final B850:B875 ratios for the three mutants, which are distinguished from one another only by the presence of a wild-type (WT) or truncated PufX (PufXΔ12) or its absence (PufX$^-$). In particular, a lower rate of LH2 assembly is observed in the PufX$^-$ LH2$^+$ mutant, as well as significantly lower final B850:B875 ratio. In contrast, the rate and extent of LH2 assembly in the PufXΔ12 LH2$^+$ strain are very similar in to those in the pseudo WT strain, with only a slightly lower B850:B875 ratio.

In view of the retarded assembly of LH2 in the PufX$^-$ LH2$^+$ mutant, we investigated the cellular levels of UPB membrane initiation sites, which sediment more slowly than mature ICM during rate-zone centrifugation on sucrose gradients [9,11,48]. A comparison of relative levels of precursor UPB membrane to mature ICM during exponential growth showed significantly lowered levels of ICM in both the PufXΔ12 LH2$^+$ and PufX$^-$ LH2$^+$ mutants, with maturation of UPB to ICM particularly affected in the absence of PufX, leading to an 8-fold accumulation of the upper band in the gradients, with respect to the PufX$^+$ control (Fig. 1C).

3.2. Analysis of pucB and puhA gene expression by quantitative PCR

In view of the lowered rate of LH2 assembly in the PufX$^-$ mutant, the levels of the *puc1B* transcript encoding the LH2 β polypeptide were measured for the PufX$^-$ LH2$^+$ and pseudo WT strains over the course of the above photosynthetic induction experiments using quantitative real-time polymerase chain reaction (Q-PCR) (Fig. 2). Levels of the *puhA* transcript, encoding the RC-H subunit, were also measured as a control. Errors in this technique are significant, so both technical and biological replicates were performed, as follows: Q-PCR assays for each time-point were performed in triplicate to give a quantifiable combined error and duplicate cultures were analysed to test reproducibility. The *pucB* and *puhA* transcript levels were normalised to those for *gyrA*, which encodes the DNA gyrase subunit

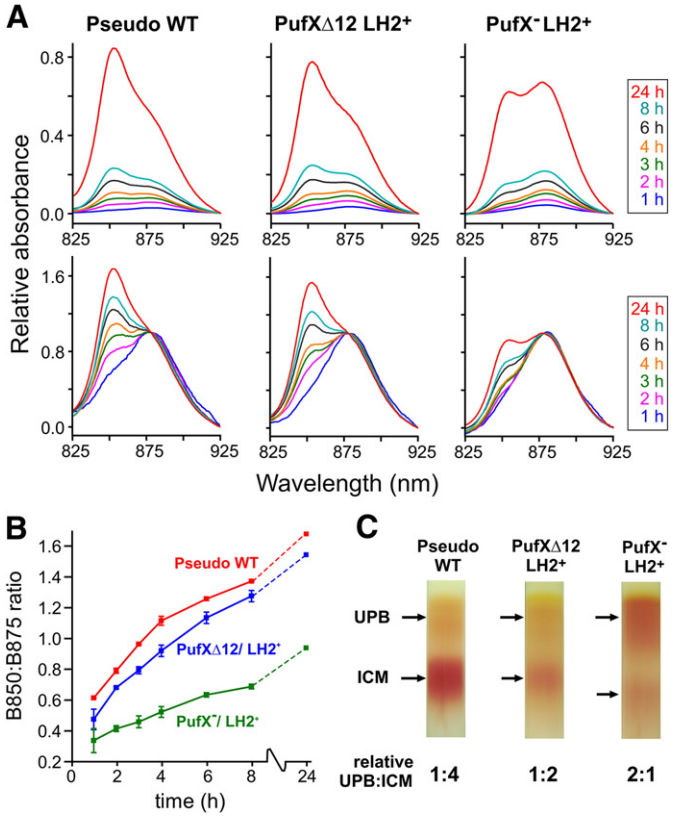

Fig. 1. Synthesis of RC–LH1 and LH2 complexes and intracellular membranes following induction of photosystem assembly under oxygen-limited conditions in the dark. (A) Time-lapse absorption spectra from cultures of three PufX-mutant strains, with samples taken at the time-points after induction specified in the insets (*right*). Spectra were analysed using Origin graphical software with baseline subtraction to remove cell scatter (t = 0 spectrum) and smoothing for clarity. *Upper row:* spectra normalised to cell density (at 680 nm). *Lower row:* spectra normalised to LH1 B875 absorbance (at 878 nm). (B) Accumulation of LH2 relative to LH1 over time, shown as the B850:B875 ratio measured from triplicate photosynthetic induction growth experiments, as in (A). Each data point is the average taken from three cultures; error bars show the mean ± standard deviation (note that some error bars are smaller than the size of the data point). (C) Photographs of sucrose gradients of photosynthetic membranes purified from the three PufX-mutant strains. The upper pigmented band (UPB) comprised of precursor membranes was compared with the lower pigmented band of mature intracytoplasmic membranes (ICM). The relative level of UPB:ICM was estimated by measuring the approximate 850 nm absorbance units harvested, which underestimates the amount of UPB, given the lack of LH2 complexes in this membrane.

A, a 'housekeeping' gene with a constant level of expression under different cellular conditions (Fig. 2, *left* and *middle*). The *pucB:puhA* ratio was analysed (Fig. 2, *right*), which describes the expression of *pucB* relative to *puhA*, rather than *gyrA*, and is thus a further comparative measure of LH2 gene expression.

For all cultures, the *pucB:gyrA* transcript ratio increases over the 8-hour time-course of the experiment with a steeper increase over the first hour of induction. The *puhA:gyrA* transcript ratio also increases sharply over the first hour, but then drops to approximately half of this level after another three hours. The *pucB:puhA* transcript ratio for all cultures increases significantly over the time-course, consistent with data described in Section 3.1 showing the preferential assembly of core complexes relative to LH2 in the early stages of photosynthetic membrane development. The results also show that, within the error of the technique, there is no significant difference in expression of *pucB* and *puhA* between the PufX$^-$ LH2$^+$ and pseudo WT strains. This implies that altered gene expression cannot account for lowered levels of LH2 complexes in the PufX$^-$ mutant.

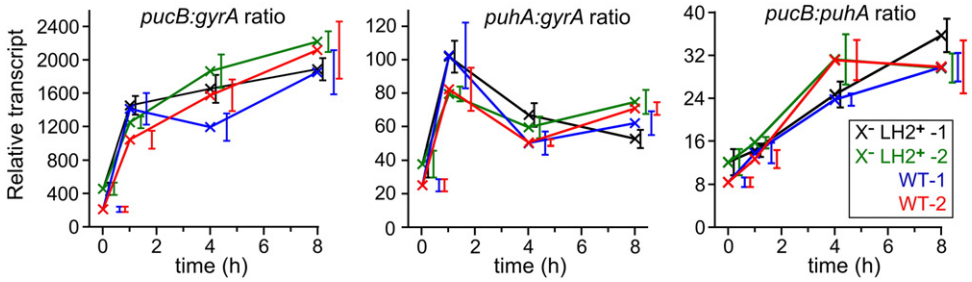

Fig. 2. Analysis of *pucB* and *puhA* gene expression by quantitative real-time PCR. In each graph duplicate cultures of the PufX$^-$ LH2$^+$ strain (*black*, *green*) and the pseudo WT strain (*blue*, *red*) were compared. Error bars show the combined standard error for each data point, determined in triplicate (technical replicates); these are offset to the right of their corresponding data point for clarity. The graphs show the relative level of the *pucB* (*left*) and *puhA* (*middle*) transcripts, each normalised to *gyrA* control transcript and the quantitative ratio of *pucB* to *puhA* transcripts (*right*), over an eight-hour time course during a photosynthetic induction growth.

3.3. Transmission electron microscopy shows that PufX$^-$ mutants have enlarged intracytoplasmic membranes

To compare the ultrastructural differences between whole cells of the PufX mutants, thin sections (60–90 nm) were taken and imaged with negative-stain TEM. The sections show that in all the three strains the cytoplasm is packed with vesicles, but that vesicle size varies (Fig. 3). In the pseudo WT, the vesicles ranged from 35 to 45 nm (Fig. 3A), comparable to previous EM studies of the true wild-type [49]. In the PufXΔ12 LH2$^+$ strain, larger vesicles were observed: of all vesicles counted, the majority were 40–55 nm and approximately 5% were significantly larger, at 70–150 nm (Fig. 3B and C). In the PufX$^-$ LH2$^+$ strain, even larger vesicles are observed, with over 15% between 70 and 150 nm. It should be noted that measurements from sectioning are underestimates of the native sizes, due to technical limitations, including the low resolution, which is limited by the fixation process and the pooling of the stain. Furthermore, the cell sections are only 90 nm thick so they might not show the maximum diameter of any given vesicle.

Purified ICM vesicles were imaged with negative-stain TEM. During preparation for TEM, samples are dried onto carbon grids and thus vesicles flatten down onto the surface, therefore these measurements, whilst being accurate, greatly overestimate the *in vivo* diameter of a vesicle, by a factor of up to two. Vesicles from pseudo WT cells were typically 100 nm wide (Fig. 4A), in agreement with previous measurements on true wild-type vesicles [9]. Vesicles from both the PufX$^-$ LH2$^+$ and PufXΔ12 LH2$^+$ mutants were regularly much larger, up to 400 nm wide (Fig. 4B and C).

Unexpectedly, in the PufX$^-$ LH2$^+$ mutant, some vesicles were found in which hexagonal patterning was observed. One such vesicle is shown in Fig. 4C, where circular features that seem to be monomeric core complexes are just visible in the raw data. A Fourier transform of the micrograph (Fig. 4C, inset) indicates that ordering was good but not perfect; the stretching of the Fourier spots in this inset is suggestive a double layer of semi-crystalline complexes. A magnification of the Fourier-filtered image clearly shows some domains of hexagonally-packed complexes (Fig. 4E). The period of the lattice is 12.5 nm, as expected for tightly-packed monomeric core complexes. This ordering is comparable to that observed for vesicles from a PufX$^-$ LH2$^-$ double-deletion mutant (Fig. 4D and F), in which hexagonally-packed monomeric core complexes have been previously defined [31].

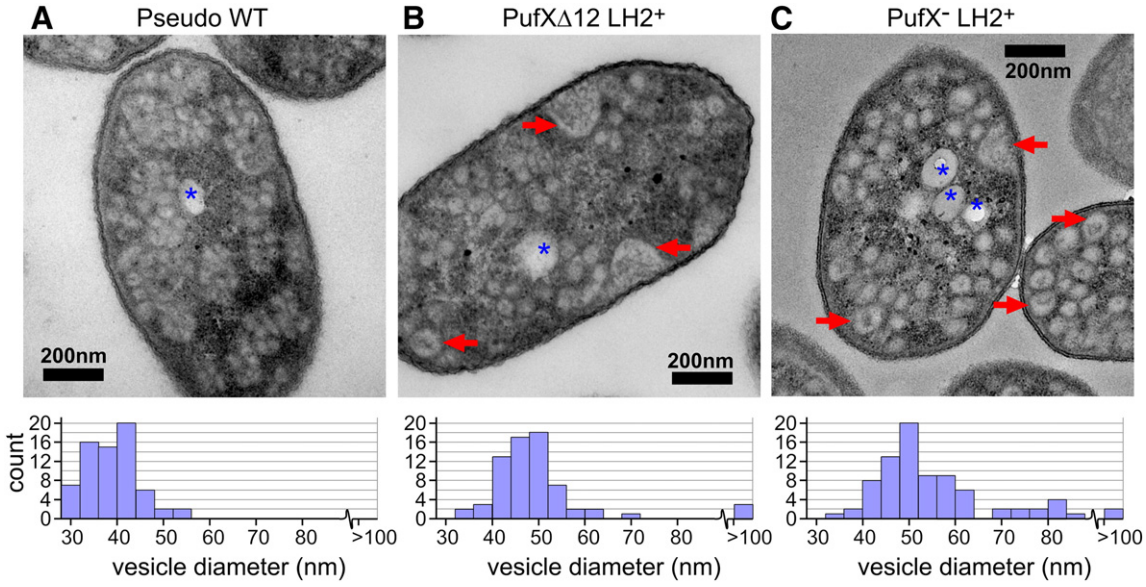

Fig. 3. Comparison of the sizes of ICMs in thin sections of cells. Comparison of the three strains: (A) pseudo WT (B) PufXΔ12 LH2$^+$ and (C) PufX$^-$ LH2$^+$. *(Top):* TEM micrographs of negatively-stained thin sections (60–90 nm) of fresh cells. Examples of particularly large vesicles are denoted by *red arrows* in (B) and (C). Storage granules were also observed (*blue asterisks*). *(Bottom):* Graphical analysis of the diameter of vesicles from cells in the above micrographs and others, n = 68, n = 68, n = 81, respectively.

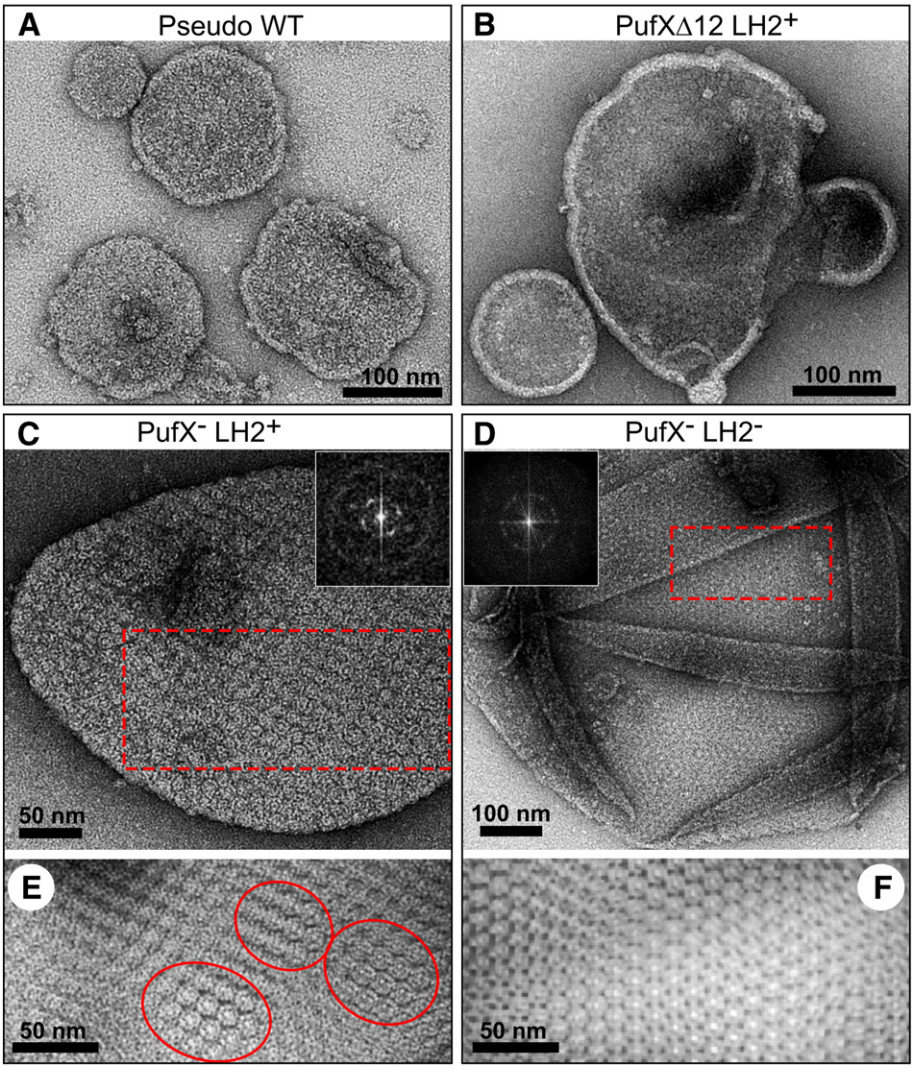

Fig. 4. TEM micrographs of negatively-stained ICM vesicles purified from PufX-mutant strains. Flattening of the samples as they are dried onto carbon grids overestimate the *in vivo* diameter of a vesicle, by a factor of up to two. (A) Pseudo WT: small vesicles of approximately 100 nm size were observed. (B) PufXΔ12 LH2$^+$ mutant: vesicles ranging from 100 to 400 nm were found. (C) PufX$^-$ LH2$^+$ mutant: a magnification of a portion of a vesicle showing hexagonal ordering. Fourier transform (*inset*), box width = 0.60 nm^{-1}. (D) PufX$^-$ LH2$^-$ mutant: a collapsed vesicle showing hexagonal ordering. Fourier transform *inset*), box width = 0.45 nm^{-1}. (E) Fourier-filtered image of the boxed area (*red*) in (C). Likely domains of core complexes are ringed (*red*). (F) Fourier-filtered image of the boxed area (*red*) in (D).

3.4. Atomic force microscopy shows evidence of core complex clustering in PufX$^-$ membranes

Purified ICM preparations were treated with very low concentrations of β-DDM (0.01 or 0.02% w/v), to gently open the vesicles so that they could be adsorbed to mica as single layers suitable for AFM. Fig. 5 panels A-D show a comparison of medium-resolution AFM topographs from different PufX mutants, in a genetic background either with or without LH2. Height profiles 1–5 allow height data to be analysed more clearly and core complexes are identified by their protruding RC-H subunits which reach heights of 7.5–8.5 nm above the mica surface, seen as prominent *white dots* in AFM topographs at this resolution.

The control pseudo WT membrane (Fig. 5A) had an organisation of photosynthetic complexes as previously described for true wild-type [7], with rows of dimeric core complexes (*blue asterisks*) interspersed by LH2, and also with some LH2-only regions (*green arrows*). This membrane patch, which was representative of the sample, was small and retained highly curved regions (the diffuse white areas) that had not fully adsorbed onto the mica. The finding of WT-like membrane architecture allows us to be confident that our plasmid-based mutation system has no substantive effect on the protein organisation.

We determined the presence or absence of dimeric core complexes by measuring the centre-to-centre distance between RC-H subunits in AFM topographs, which is 7.8 nm in patches of ICM on mica [9]. Distances in excess of this value are likely to indicate the presence of monomeric core complexes. PufX$^-$ LH2$^-$ membranes, which TEM has previously shown to be comprised solely of hexagonally-packed monomeric core complexes [31], were imaged by AFM as a further control. In these we measured an RC–RC period of 12.1 nm (Fig. 5D). In the PufX$^-$ LH2$^+$ mutant, some membranes were found with regions of hexagonally-packed monomeric core complexes (Fig. 5C, *ringed*), with a measured RC–RC separation of 12.4 nm. This is consistent with the hexagonal packing observed in our TEM data (Fig. 4C). PufXΔ12 LH2$^+$ membranes (Fig. 5B) did not contain any dimeric core complexes despite the presence of the PufX polypeptide in its truncated form, nor did we observe any large areas that consisted entirely of core complexes. Although LH2 rings are not well resolved in these images, LH2-only regions were observed only in Fig. 5A, when core dimers were present.

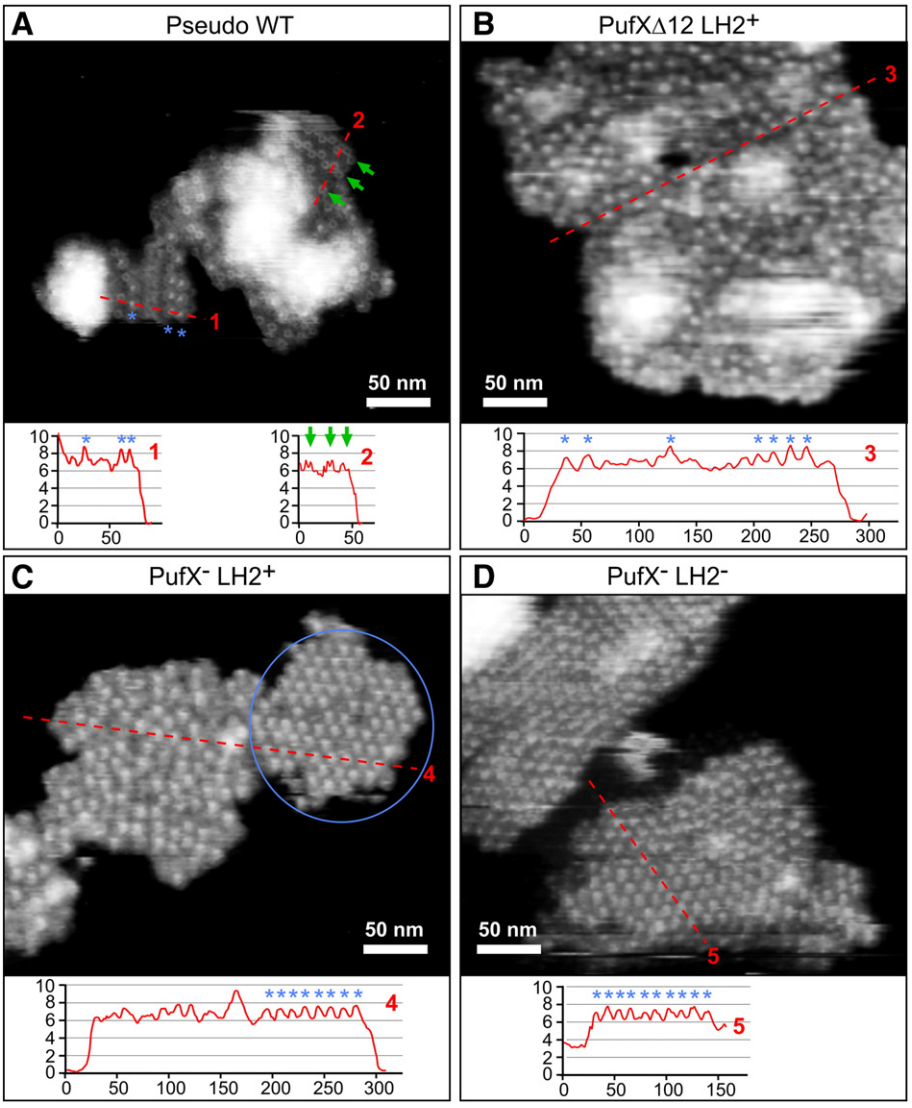

Fig. 5. Medium-resolution AFM showing evidence of core complex clustering. AFM topographs of PufX-mutant membranes, all to equal scale; the full z-range (greyscale) is 15 nm. Height profiles (*red*) are measured across areas of interest, with axes in nm. (A) Pseudo WT membrane. Dimeric core complexes (**), monomeric core complexes (*) and zigzag patterns of LH2 (*arrows*) were observed. Note that the highly curved regions above 15 nm are above the z-scale displayed here. (1) Height profile through a monomeric core complex (*) then a dimeric core complex (**) which had an intra-dimer RC–RC separation measured as 7.8 nm. (2) Height profile through an LH2-only region. *Arrows* denote high LH2 rings within the high-low zigzag arrangement. (B) PufXΔ12 LH2$^+$ membrane. A moderately-high density of core complexes was found (represented by highly protruding RC-H subunits). (3) Height profile through the membrane fragment, intersecting many core complexes (*). (C) PufX$^-$ LH2$^+$ membrane. A high density of core complexes was observed. In the top-right region (*ringed*) hexagonally-ordered core complexes were observed. (4) Height profile through disordered core complexes and LH2, then a row of eight hexagonally-ordered core complexes (*) with periodic RC–RC separation of 12.4 nm. (D) PufX$^-$ LH2$^-$ membrane. All observable core complexes were found in hexagonally-packed lattices. (5) Height profile through a row of ten hexagonally-ordered core complexes (*), with a periodic RC–RC separation of 12.1 nm.

3.5. Quantitative analysis of mixed domains of core monomers and LH2 complexes in membranes from PufX mutants using high-resolution atomic force microscopy

At high resolution, core complexes were clearly defined as LH1 rings surrounding the central RC subunits and LH2 complexes as the smaller rings (without a central density). The pseudo WT membrane will not be discussed further, except to say that in higher resolution images dimeric core complexes and LH2-only areas are more clearly defined (Fig. S1) and that the wild-type arrangement [7] is clearly maintained. High-resolution AFM analysis of PufXΔ12 LH2$^+$ and PufX$^-$ LH2$^+$ membranes is shown in Fig. 6. For colour 3-D representations and analysis of entire membrane patches, see Fig. S2. Statistical analysis of the AFM data is shown in Tables 1–3, where as many well-resolved LH complexes as possible were measured.

The AFM topographs show that the membranes are packed with LH complexes, with core complexes clustered together. To definitively test whether the core complexes are 100% monomeric, RC–RC separations between neighbouring core complexes were measured (Table 1). For PufX$^-$ and PufXΔ12 cores, the RC–RC separation was 12.3 ± 0.9 nm (n = 56) and 12.4 ± 0.8 nm (n = 56), respectively, in contrast to the significantly smaller intra-dimer RC–RC separation of 8.1 ± 0.4 nm (n = 14) in the pseudo WT control. The relatively high standard deviations for these values may reflect rotation of the RC within the LH1 ring, as previously described in AFM of *Rhodopseudomonas (Rps.) viridis* core complexes [50]. Nevertheless, these 'minimal' RC–RC distances between neighbouring complexes found here in both PufX$^-$ and PufXΔ12 cores correlate well to those from hexagonally-packed monomeric core complexes [31] (Figs. 4C-F, 5C and D) thus we conclude they are monomeric in all cases.

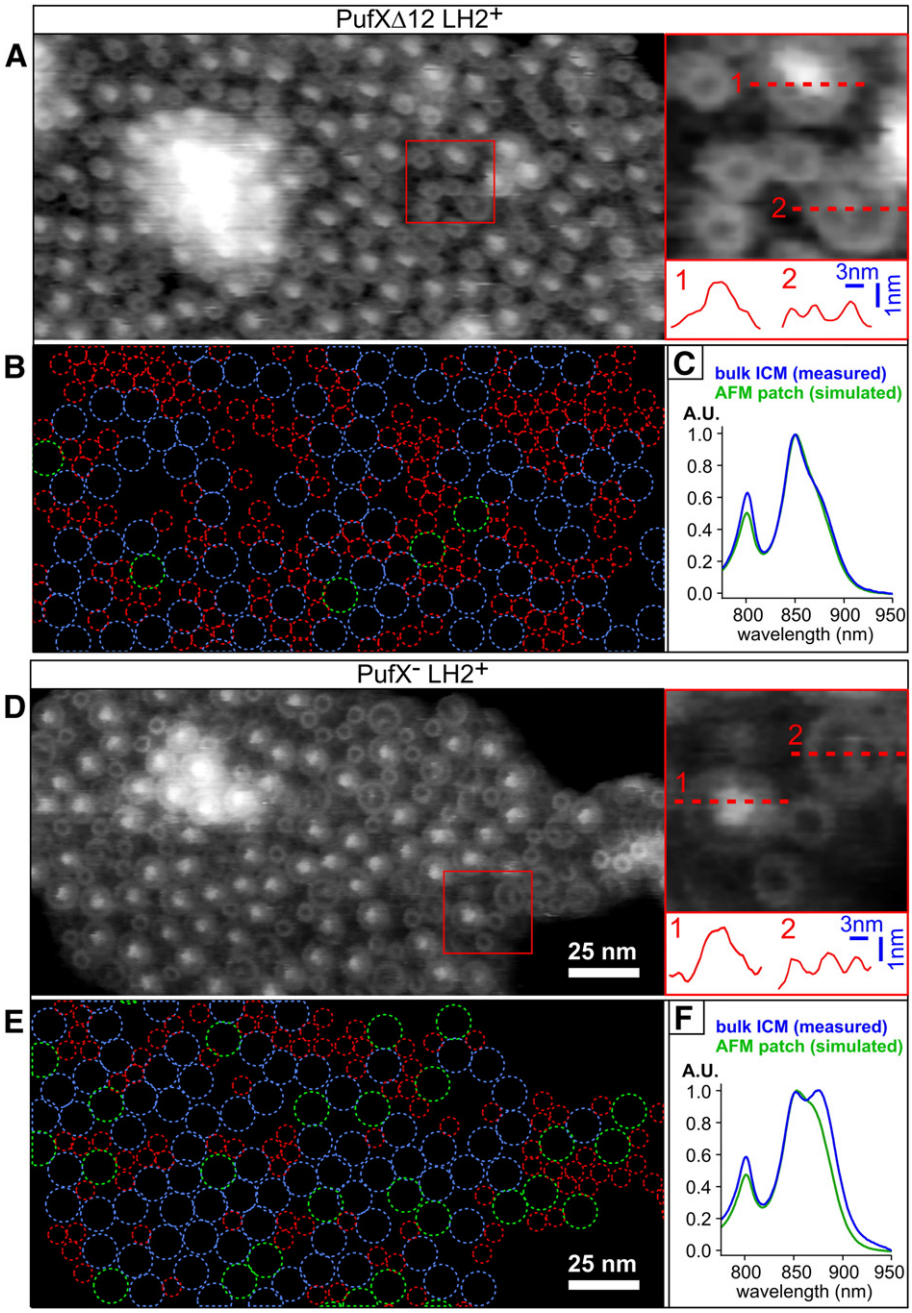

Fig. 6. High-resolution AFM analysis of PufX mutant membranes. AFM topographs of a membrane fragment from (A) PufXΔ12 LH2$^+$ and (D) PufX$^-$ LH2$^+$ mutants. Both topographs are to an equal scale, with the x–y scale bar shown in (D); the full z-range (greyscale) is 15 nm. (*Inset* A, D): magnification of part of the image (*boxed red*), with increased contrast for clarity. In each inset, height profiles (*red*) are shown of (1) a core complex with an intact RC and (2) a core complex lacking the RC-H subunit. (B), (E): assignment of all clearly distinguishable complexes, from topographs (A) and (D) respectively, as either LH2 (*red*), intact core complexes (*blue*) or core complexes lacking the RC-H subunit (*green*). (C), (F): Comparison of absorbance spectrum measured from the bulk ICM sample (*blue*) and a simulated absorbance spectrum (*green*) based on the numbers of LH2 and core complex counted in the AFM topograph (see Section 2.9). Spectra aligned at 925 nm and normalised at 850 nm for clarity.

Upon close inspection of the core complexes in both images, two distinct types are clearly found; those with an intact RC and those where the RC-H subunit has been removed by the AFM probe (Fig. 6A and D, *insets*). This sort of probe-induced 'nano-dissection' of the core complex has been reported for crystals and membranes from other purple bacteria [50–52] but not previously for *Rba. sphaeroides* membranes. Fig. S3 shows the progressive removal of RC-H subunits over sequential images. This nano-dissection of the RC allowed measurement of the underlying features and clearer definition of the LH1 ring. Note that the PufX$^-$ LH2$^+$ topograph is at slightly higher resolution and is therefore clearer than the PufXΔ12 LH2$^+$ topograph, so further analysis was focused on this sample. Measurements of the dimensions of core complexes were made, comparing those with RCs intact and those where the RC-H subunit has been removed. (Table 2). The LH1 ring is clearer in the RC-H-removed cores, and the rings show only a very slight random tilt. In the RC-intact cores the left hand-edge of the LH1 ring ('edge 1' in the left-to-right trace direction of scanning) is clearly defined, but the right-hand edge ('edge 2') is slightly obscured by scanning over the highly protruding RC-H, therefore 'edge 1' data were used in height analyses of intact cores. The LH1 ring height and diameter were consistent between the RC-intact and RC-H-removed complexes, thus we are confident that there

Table 1
Statistical analysis of high-resolution AFM topographs: comparison of the minimal RC–RC separation between the different PufX mutants. For all lateral measurements the 'peak–peak' separation was measured (see Section 2.9). All mean and standard deviation (s.d.) measurements in nanometers. AFM has higher accuracy in the z-direction than the x- and y-directions, therefore height measurements are to two decimal places and lateral measurements are to one decimal place. For the pseudo WT, the RC–RC separation was the RC to RC distance within potential dimeric core complexes ('intra-dimer'). For both the PufXΔ12 LH2$^+$ and the PufX$^-$ LH2$^+$ mutants, this was the RC to RC distance between neighbouring core complexes ('inter-monomer').

System	RC–RC separation		
	Mean	s.d.	n
Pseudo WT control: intra-dimer	8.1	0.4	14
PufXΔ12 LH2$^+$: inter-monomer	12.4	0.8	56
PufX$^-$ LH2$^+$: inter-monomer	12.3	0.9	56

is no damage to the extrinsic parts of the LH1 complex during nano-dissection. The protrusion of RC-H above the LH1 ring is measured here as 1.68 ± 0.22 nm (n = 26), slightly lower than that previously reported for the *Rhodospirillum (Rsp.) rubrum* core complex [51].

It has been previously reported that upon flattening of the natively-curved membrane onto the mica substrate for AFM, LH2 is displaced to high and low registers within the membrane, forming zigzag arrangements in LH2-only and wild-type membranes [7,37] (Fig. 5A). In the PufX$^-$ and PufXΔ12 membranes LH2 complexes are packed in clusters between core complexes, and rather than zigzags other hexagonal high-low arrangements are found. The dimensions of high- and low-register LH2 complexes were compared (Table 3). The measured diameter of the LH2 ring was very similar between the high and low forms, 4.8 ± 0.3 nm (n = 34) and 4.9 ± 0.2 nm (n = 19), respectively, showing with high accuracy that the LH2 complexes are essentially the same at both levels. The height from the mica surface of high- and low-register LH2 was measured as 6.75 ± 0.15 nm (n = 21) and 5.85 ± 0.11 nm (n = 13), respectively, hence the 'high' form is approximately 0.90 nm above the 'low' form, in agreement with the data of Olsen and co-workers recorded on LH2-only membranes [37]. Our measured LH2 ring diameter and height compare favourably with the X-ray structure of LH2 from *Rps. acidophila* [53] and with a previous AFM analysis of 2D crystals of *Rba. sphaeroides* LH2 [54].

The high resolution allows identification of almost the entire area of the membrane as either core complexes (RC-intact or RC-H-removed) or LH2 (Fig. 6B and E). Gaps in the assigned area allow sufficient space for other essential photosynthetic proteins that have not been thus far identified by AFM. The overall compositions were as follows: 366 LH2 and 181 core complexes (including 11 RC-H-removed) for the PufXΔ12 LH2$^+$ membrane and 121 LH2 and 122 core complexes (including 33 RC-H-removed) for the PufX$^-$ LH2$^+$ membrane. This leads to core/LH2 ratios of 0.49 and 1.01, respectively. To test the correspondence of the membrane imaged by AFM to the original sample of purified ICM vesicles, absorbance spectra of these particular membrane patches were simulated (Fig. 6C and F). Spectra were generated as described in Section 2.9, by arithmetic combination of the absorbance spectrum of core complex-only membrane (B875 only) and the spectrum for LH2-only membrane (B800–850 only) in the ratios determined above, factoring in the measured extinction coefficients of the protein complexes. The simulated spectra for the PufXΔ12 LH2$^+$ and PufX$^-$ LH2$^+$ membranes have 875/850 nm absorbance ratios of 0.60 and 0.84, respectively, as compared with the 875/850 nm absorbance ratios measured for the ICM samples of 0.63 and 1.01. The simulated spectrum of the PufXΔ12 LH2$^+$ membrane corresponds very closely to the absorbance spectrum measured from the bulk ICM sample, giving us confidence this that AFM image is representative of the starting membrane sample. The simulated spectrum of the PufX$^-$ LH2$^+$ membrane has a significantly lower 875/850 nm absorbance ratio than the bulk ICM spectrum, and therefore contains fewer core complexes per LH2 than may be expected. This reflects the partial segregation effect described in Section 3.4; the 'missing' B875 represents those core complexes that have partitioned into core-only domains, which have become disconnected from the membrane patches.

Table 2
Statistical analysis of high-resolution AFM topographs: measurement of the dimensions of PufX$^-$ core complexes. Details of measurements as for Table 1. Intact core complexes are compared with those where the AFM probe has dissected the RC, removing the RC-H subunit. Due to slight imperfections in tracking the trailing edge whilst scanning over the protruding RC-H subunit the LH1 edge 2 height seems to be very slightly overestimated (*), therefore the LH1 (edge 1) height for RC-intact cores was used to calculate the RC protrusion.

Parameter	Core (RC-H-removed)			Core (RC-intact)		
	Mean	s.d.	n	Mean	s.d.	n
LH1 height (edge 1)	6.65	0.24	10	6.70	0.18	16
LH1 height (edge 2)	6.75	0.20	10	7.03*	0.26	16
LH1 height (average)	6.70	0.17	10	6.86*	0.17	16
LH1 diameter (peak–peak)	9.8	0.3	15	9.7	0.40	26
RC protrusion (above LH1)	0.26	0.11	15	1.68	0.22	26

Table 3
Statistical analysis of high-resolution AFM topographs: measurement of the dimensions of LH2 complexes from the PufX$^-$ LH2$^+$ strain. Details of measurements as for Table 1. 'High' and 'low' refer to the displacement of LH2 complexes to high and low registers within the membrane, which results from flattening of curved membranes onto the mica substrate for AFM.

Parameter	LH2 (high)			LH2 (low)		
	Mean	s.d.	n	Mean	s.d.	n
LH2 height (edge 1)	6.69	0.19	21	5.90	0.14	13
LH2 height (edge 2)	6.81	0.15	21	5.81	0.16	13
LH2 height (average)	6.75	0.15	21	5.85	0.11	13
LH2 diameter (peak-peak)	4.8	0.3	34	4.9	0.2	19

4. Discussion

4.1. Retarded LH2 assembly in the PufX$^-$ mutant, but not in the PufXΔ12 mutant: local membrane curvature favours stable assembly of the LH2 complex

We have found a reproducible and significant decrease in the LH2 content of the PufX$^-$ mutant, which must reflect an effect on LH2 assembly at some level, from transcription of the cognate *puc* genes onwards. This reduction in LH2 content was noticed in earlier work, but could not be explained [38]. We have undertaken a systematic survey of the possible origins of this PufX effect by measuring levels of *puc* transcripts and LH2 incorporation during induction of membrane assembly, as well as the morphology of the ICM and the membrane organisation of the core and LH2 complexes. Apart from the two extremes of strains with or without PufX, which assemble dimeric or monomeric RC–LH1 core complexes respectively [30–32], we also studied the intermediate case of the PufXΔ12 mutant which has a 12-residue truncation of the N-terminus that results in monomeric, PufX-containing core complexes [32].

Analysis of the first two hours of membrane induction showed that the PufX$^-$ mutant assembles LH2 into ICM over three-fold more slowly than the PufX$^+$ pseudo WT control (Fig. 1A and B), so after 60 min of membrane assembly the PufX$^-$ LH2$^+$ mutant is almost entirely comprised of B875 (see Fig. 1A, bottom-right graph). Slightly surprisingly, the rate of LH2 assembly in the PufXΔ12 mutant resembles the rate seen in the pseudo WT control rather than that in the PufX$^-$ mutant, showing that LH2 incorporation does not relate to the presence of core monomers or dimers in a simple way. This point will be returned to later.

Q-PCR showed that there is no discernible difference between levels of *puc* gene expression between the pseudo WT and PufX$^-$ LH2$^+$ cells (Fig. 2). Even taking into account the uncertainty due to the errors inherent in this technique, these levels of gene expression would not account for the difference in spectroscopically observed LH2 in the membrane. Therefore, we expect that the difference in amounts of LH2 within the mature membranes of these strains arises from an effect of PufX at the level of protein assembly.

From previous work on membrane assembly in *Rba. sphaeroides* it is known that formation of ICM is initiated at curved regions of the cytoplasmic membrane, which can be isolated as a slowly sedimenting membrane fraction when French-pressed extracts of cells are analysed by rate-zone centrifugation [9,11,54]. One characteristic of these 'early' UPB membranes is the relative lack of LH2, and moreover these low levels of complex appear to be poorly connected to the core complexes [9,14]. A previous study has shown that incorporation of PufX, a necessary precondition for dimer formation, occurs before LH1 assembly [55]. Thus, ICM formation appears to be a two-stage process with early incorporation of PufX and formation of core dimers tending to precede the formation of LH2 domains. Analysis of the proportions of UPB and ICM in PufX$^+$, PufXΔ12 and PufX$^-$ strains shows that maturation of UPB has been arrested, leading to an accumulation of UPB membrane and reduced formation of fully invaginated ICM. The most obvious explanation is the reduced rate and extent of LH2 assembly, which is required to drive the further invagination of UPB regions.

Tucker and co-workers [9] proposed that stable assembly of the LH2 complex is aided by the pre-curving of the membrane by the developing dimeric core arrays. Why then would the PufXΔ12 LH2$^+$ mutant, shown by AFM to contain monomeric core complexes, have rates of LH2 assembly more typical of the PufX$^+$ pseudo WT control, rather than the PufX$^-$ LH2$^+$ mutant? We propose that transient associations of PufXΔ12 core complexes in the ICM mimic the structure of the WT core dimer and locally distort the membrane, temporarily favouring LH2 assembly. Such transient, local distortions of a membrane have been simulated using the Molecular Dynamics Flexible Fitting (MDFF) method, performed on the RC–LH1–PufX dimer housed in a 32×17 nm patch of lipids [24]. The MDFF experiment revealed a spontaneous curvature of the WT core dimer, and after 29 ns of the simulation the entire lipid patch became arched as a consequence of the bending of the dimer. This process was accompanied by a twisting of the dimer, which, together with an offset that aligned their curvature axes, resulted in core dimers that could stack along their long axes forming tubular membranes, in agreement with the packing of core dimers in tubular membranes of an LH2$^-$ mutant measured by EM [23]. WT or PufXΔ12 molecules apparently distort the LH1 ring on the periplasmic side of the membrane to give a slightly wedge-shaped complex (Fig. 7). The fact that the dimer has 14 + 14 LH1 αβ pairs, as opposed to the 16 + 16 αβ pairs found in two PufX$^-$ core monomers, provides some 'room' for this distortion. In the core dimer this modified conformation of two RC–LH1–PufX monomers allows a stable 146° bend in the complex to form, locked in place by the N-terminal domains of the PufX polypeptides on opposing sides of the core dimer (Fig. 7). In the intermediate case of the PufXΔ12 LH2$^+$ mutant the conformation of each monomer LH1 ring resembles that in the dimer, without the capacity to form a permanent link driven by the PufX N-terminus, so that dimers can still form, although only transiently. In the absence of PufX, the LH1 ring relaxes to form a more cylindrical shape which promotes the formation of planar membrane sheets containing RC–LH1 monomers.

The hypothesis presented in Fig. 7 suggests that stable assembly of LH2 complexes is optimised in membranes where microdomains of RC–LH1–PufX complexes form as a result of the interactions driven by the shape and curvature mismatch factors identified by the Monte Carlo simulations [38], which co-operatively bend the membrane. We suggest that because of the retained shape of the PufXΔ12 monomers there is a transient formation of core dimers in the PufXΔ12 LH2$^+$ mutant, sufficient to create the conditions for efficient LH2 insertion and assembly. LH2 assembly is less favoured in the more planar membranes that house PufX$^-$ core complexes.

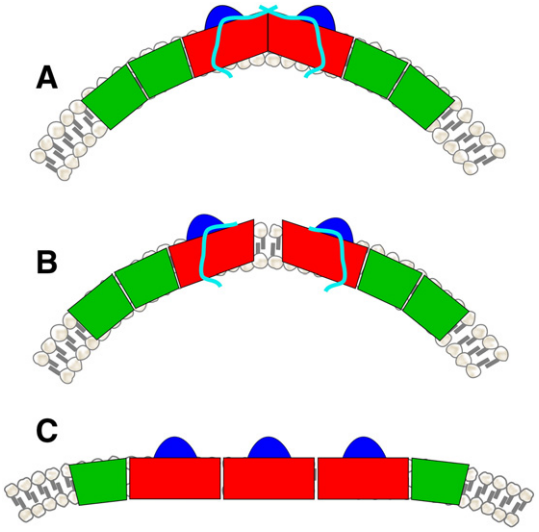

Fig. 7. Diagrammatic models for the effects of the (A) PufX$^+$, (B) PufXΔ12 and (C) PufX$^-$ core complexes on membrane curvature, domain formation and LH2 insertion. RCs are in blue, LH1 in red and LH2 complexes in green. PufX is represented by a cyan line. (A) Dimeric core complexes, stabilised by the N-terminal interactions of PufX molecules from opposing halves of the dimer, impose curvature on the membrane, which favours the stable assembly of LH2 complexes. (B) represents the intermediate case of the PufXΔ12 LH2$^+$ mutant, where the conformation of each monomer LH1 ring resembles that in the dimer, without the capacity to form a permanent link driven by the PufX N-terminus. The transient formation of dimers is proposed, which favours LH2 assembly due to local curvature of the membrane. In the PufX$^-$ mutant in (C) the LH1 ring relaxes to form a more cylindrical shape which promotes the formation of planar membrane sheets containing RC–LH1 monomers. These core monomers cluster within the membrane to form hexagonally ordered domains, and the more planar membrane is less favourable for stable assembly of LH2 complexes.

4.2. The effect of PufX in promoting lateral sorting of photosynthetic complexes into membrane domains

The formation of bent RC–LH1–PufX core dimers imposes curvature on the membranes that house these dimers [23,24], and there are also consequences for the organisation of core and LH2 complexes into domains. AFM shows that RC–LH1–PufX dimers and LH2 complexes partition into core- and LH2-enriched regions (Fig. 5A and [7]), in agreement with linear dichroism (LD) analyses of ICM [8,38]. Monte Carlo simulations were carried out which modelled the dynamic interactions of photosynthetic complexes using an approach developed for analysing the behaviour of colloids [38]. These simulations took into account the size asymmetry between core and LH2 complexes, as well as different degrees of curvature mismatch that result when LH2 interacts with the angled outside face of a core dimer or with the perpendicular outside face of a PufX$^-$ core monomer. The results of these simulations showed that a general mechanism promotes the formation of dimer-only and LH2-only domains in wild-type membranes of *Rba. sphaeroides*, also applicable to the formation of specialised domains in other biological membranes. The colloid model also predicts a weaker but still significant driving force for domain formation even when core monomers and LH2 are present, since there is still a size asymmetry, even though there is no curvature mismatch. This prediction is borne out by the Fourier analysis of the TEM image of the PufX$^-$ LH2$^+$ mutant which shows that hexagonally-packed domains are present (Fig. 4C and E) with lattice dimensions similar to those measured from the PufX$^-$ LH2$^-$ control strain (Fig. 4D and F), showing a RC–RC separation of

~12.5 nm. We conclude that these are domains composed entirely of core monomers, from which LH2 has been excluded. Further support for the existence of core monomer-only regions is provided by AFM data (Fig. 5C), which clearly shows such a region (blue circle), with a measured RC–RC separation of 12.4 nm.

The AFM topograph in Fig. 5C also shows that ordered and disordered RC–LH1 domains can co-exist, supporting the LD data of Frese and co-workers [38], which also showed that PufX$^-$ LH2$^+$ membranes partition into such domains. The surprising aspect of their LD study was that in approximately half of the membranes in the sample they observed a defined orientation of the RC within the LH1 ring, whether or not PufX was present. This was proposed to be driven by lateral packing forces in the membrane plane that, perhaps only transiently, induce a configuration of the flexible LH1 ring, which is transmitted to the enclosed RC. Since the RCs in a domain are roughly elliptical in cross section, they respond to external, directional deformation of the LH1 rings by rotating in a particular direction, which produces the observed LD signal.

4.3. Evidence from analysis of high-resolution AFM topographs that PufX stabilises the core complex

A detailed analysis of high-resolution AFM data (Fig. 6, Fig S2) demonstrates that that in both PufXΔ12 and PufX$^-$ mutants, the core complexes are monomeric, the closest RC–RC distances between proposed monomers being 12.4 ± 0.8 and 12.3 nm ± 0.9 nm, respectively (n = 56 for both), compared to an intra-dimer RC–RC separation of 8.1 nm (n = 14) (Table 1). In the PufX$^-$ mutant we assume that core complexes are comprised of a closed circular ring of sixteen LH1 αβ pair around the RC, analogous to the *Rsp. rubrum* complex [56]. For the PufXΔ12 mutant, where it is known that the truncated PufX is present within the monomeric core complex [32], we postulate a fifteen LH1 αβ pair 'open' ring with the truncated PufX, analogous to the *Rps. palustris* RC–LH1–PufW complex [57].

The measurements of LH1 ring height and RC-H protrusion (Table 2) are slightly lower than those described in a model for the *Rsp. rubrum* core complex [51]. These differences could suggest that in the non-native, PufX-deficient *Rba. sphaeroides* monomer, the RC relaxes more deeply into the LH1 ring. Additionally, our measured LH1 ring diameter corresponds very closely to the length measured for the long axis of elliptical *Rps. palustris* cores in a previous AFM analysis [52], so it seems plausible that the PufX-deficient LH1 complex may be less tightly packed around the RC, forming a more relaxed, larger ring. In pseudo WT membranes, disturbance of the RC was rare (Fig. S1), whereas in the PufX mutants 'nano-dissection' of the core complex, with removal of the RC-H subunit (Fig. 6, Fig. S3), was common. This observation suggests that the PufX-deficient core complex monomer is less stable than the native dimer.

5. Conclusion

Lower rates of LH2 assembly and retarded maturation of membrane invagination were observed in a PufX$^-$ mutant with reduced membrane curvature, leading to the proposal that in the wild-type bent RC–LH1–PufX dimers deform ICM and create a favourable environment for stable assembly of LH2 complexes. In the wild-type there are three types of mismatch between core dimer and LH2 complexes, in terms of curvature, size and shape [38], which tend to drive the formation of locally curved core- and LH2-enriched membrane domains. One consequence of creating PufX$^-$ core monomers is to confine the mismatch between cores and LH2 to one of size only, which in turn alters the driving forces for membrane curvature and domain formation. Thus, in PufX$^-$ mutants some partitioning of complexes is retained, with core monomers partitioning into hexagonally packed clusters, but the reduced degree of membrane curvature is less favourable for optimal rates of LH2 assembly. We suggest that the observation of near-normal rates of LH2 assembly in a mutant with monomeric cores, but with an N-terminally truncated PufX, arises from transient core monomer–monomer associations that produce temporary, local membrane curvature, with the consequence that efficient LH2 assembly is still possible. These observations highlight the influences of membrane fluidity and protein mobility on membrane assembly, organisation and function.

Supplementary materials related to this article can be found online at doi:10.1016/j.bbabio.2011.05.019.

Acknowledgements

CNH acknowledges financial support from the Biotechnology and Biological Sciences Research Council (UK). CNH and JDO were supported as part of the Photosynthetic Antenna Research Center (PARC), an Energy Frontier Research Center funded by the U.S. Department of Energy, Office of Science, Office of Basic Energy Sciences under Award number DE-SC 0001035. PGA, DJM and IWN were all supported by doctoral studentships from the Biotechnology and Biological Sciences Research Council (UK). PGA and CNH would like to thank Dr Matt Rolfe and Professor Jeff Green, University of Sheffield, for helpful discussions and use of facilities relating to Q-PCR.

References

[1] R. van Grondelle, J.P. Dekker, T. Gillbro, V. Sundström, Energy-transfer and trapping in photosynthesis, Biochim. Biophys. Acta, Bioenerg. 1187 (1994) 1–65.
[2] M. Sener, J. Strumpfer, J.A. Timney, A. Freiberg, C.N. Hunter, K. Schulten, Photosynthetic vesicle architecture and constraints on efficient energy harvesting, Biophys. J. 99 (2010) 67–75.
[3] M.K. Sener, J.D. Olsen, C.N. Hunter, K. Schulten, Atomic level structural and functional model of a bacterial photosynthetic membrane vesicle, Proc. Natl. Acad. Sci. USA 104 (2007) 15273–15278.
[4] P.A. Bullough, P. Qian, C.N. Hunter, Reaction center–light harvesting core complexes of purple bacteria, in: C.N. Hunter, F. Daldal, M.C. Thurnauer, J.T. Beatty (Eds.), The Purple Phototrophic Bacteria, Springer, Dordrecht, The Netherlands, 2009, pp. 155–179.
[5] J.N. Sturgis, J.D. Tucker, J.D. Olsen, C.N. Hunter, R.A. Niederman, Atomic force microscopy studies of native photosynthetic membranes, Biochemistry 48 (2009) 3679–3698.
[6] S. Scheuring, J. Sturgis, Atomic force microscopy of the bacterial photosynthetic apparatus: plain pictures of an elaborate machinery, Photosyn. Res. 102 (2009) 197–211.
[7] S. Bahatyrova, R.N. Frese, C.A. Siebert, J.D. Olsen, K.O. van der Werf, R. van Grondelle, R.A. Niederman, P.A. Bullough, C. Otto, C.N. Hunter, The native architecture of a photosynthetic membrane, Nature 430 (2004) 1058–1062.
[8] R.N. Frese, C.A. Siebert, R.A. Niederman, C.N. Hunter, C. Otto, R. van Grondelle, The long-range organization of a native photosynthetic membrane, Proc. Natl. Acad. Sci. USA 101 (2004) 17994–17999.
[9] J.D. Tucker, C.A. Siebert, M. Escalante, P.G. Adams, J.D. Olsen, C. Otto, D.L. Stokes, C.N. Hunter, Membrane invagination in *Rhodobacter sphaeroides* is initiated at curved regions of the cytoplasmic membrane, then forms both budded and fully detached spherical vesicles, Mol. Microbiol. 76 (2010) 833–847.
[10] C.N. Hunter, H.J.M. Kramer, R. van Grondelle, Linear dichroism and fluorescence emission of antenna complexes during photosynthetic unit assembly in *Rhodopseudomonas sphaeroides*, Biochim. Biophys. Acta 807 (1985) 44–51.
[11] R.A. Niederman, D.E. Mallon, L.C. Parks, Membranes of *Rhodopseudomonas sphaeroides*. VI. Isolation of a fraction enriched in newly synthesized bacteriochlorophyll α-protein complexes, Biochim. Biophys. Acta 555 (1979) 210–220.
[12] J. Chory, T.J. Donohue, A.R. Varga, L.A. Staehelin, S. Kaplan, Induction of the photosynthetic membranes of *Rhodopseudomonas sphaeroides*: biochemical and morphological studies, J. Bacteriol. 159 (1984) 540–554.
[13] C.N. Hunter, J.D. Tucker, R.A. Niederman, The assembly and organisation of photosynthetic membranes in *Rhodobacter sphaeroides*, Photochem. Photobiol. Sci. 4 (2005) 1023–1027.
[14] C.N. Hunter, R. van Grondelle, N.G. Holmes, O.T.G. Jones, R.A. Niederman, Fluorescence yield properties of a fraction enriched in newly synthesized bacteriochlorophyll *a* protein complexes from *Rhodopseudomonas sphaeroides*, Photochem. Photobiol. 30 (1979) 313–316.
[15] J.R. Bowyer, C.N. Hunter, T. Ohnishi, R.A. Niederman, Photosynthetic membrane development in *Rhodopseudomonas sphaeroides*. Spectral and kinetic characterization of redox components of light-driven electron flow in apparent photosynthetic membrane growth initiation sites, J. Biol. Chem. 260 (1985) 3295–3304.
[16] C.S. Young, J.T. Beatty, Topological model of the *Rhodobacter capsulatus* light-harvesting complex I assembly protein LhaA (previously known as ORF1696), J. Bacteriol. 180 (1998) 4742–4745.
[17] C.S. Young, R.C. Reyes, J.T. Beatty, Genetic complementation and kinetic analyses of *Rhodobacter capsulatus* ORF1696 mutants indicate that the ORF1696 protein

enhances assembly of the light-harvesting I complex, J. Bacteriol. 180 (1998) 1759–1765.
[18] M. Aklujkar, R.C. Prince, J.T. Beatty, The PuhB protein of *Rhodobacter capsulatus* functions in photosynthetic reaction center assembly with a secondary effect on light-harvesting complex 1, J. Bacteriol. 187 (2005) 1334–1343.
[19] L.M. Gong, J.K. Lee, S. Kaplan, The *Q* gene of *Rhodobacter sphaeroides*: its role in *puf* operon expression and spectral complex assembly, J. Bacteriol. 176 (1994) 2946–2961.
[20] D.C. Youvan, E.J. Bylina, M. Alberti, H. Begusch, J.E. Hearst, Nucleotide and deduced polypeptide sequences of the photosynthetic reaction center, B870 antenna and flanking polypeptides from *Rhodopseudomonas capsulata*, Cell 37 (1984) 949–957.
[21] L.C.D. Gibson, P. McGlynn, M. Chaudhri, C.N. Hunter, A putative anaerobic coproporphyrinogen III oxidase in *Rhodobacter sphaeroides*. II. Analysis of a region of the genome encoding *hemF* and the *puc* operon, Mol. Microbiol. 6 (1992) 3171–3186.
[22] M. Aklujkar, R.C. Prince, J.T. Beatty, The photosynthetic deficiency due to *puhC* gene deletion in *Rhodobacter capsulatus* suggests a PuhC protein-dependent process of RC/LH1/PufX complex reorganization, Arch. Biochem. Biophys. 454 (2006) 59–71.
[23] P. Qian, P. Bullough, C.N. Hunter, Three-dimensional reconstruction of a membrane-bending complex, J. Biol. Chem. 283 (2008) 14002–14011.
[24] J. Hsin, J. Gumbart, L.G. Trabuco, E. Villa, P. Qian, C.N. Hunter, K. Schulten, Protein-induced membrane curvature investigated through molecular dynamics flexible fitting, Biophys. J. 97 (2009) 321–329.
[25] J.W. Farchaus, W.P. Barz, H. Grunberg, D. Oesterhelt, Studies on the expression of the *pufX* polypeptide and its requirement for photoheterotrophic growth in *Rhodobacter sphaeroides*, EMBO J. 11 (1992) 2779–2788.
[26] W.P. Barz, F. Francia, G. Venturoli, B.A. Melandri, A. Verméglio, D. Oesterhelt, Role of the PufX protein in photosynthetic growth of *Rhodobacter sphaeroides*. 1. PufX is required for efficient light-driven electron transfer and photophosphorylation under anaerobic conditions, Biochemistry 34 (1995) 15235–15247.
[27] J.W. Farchaus, H. Gruenberg, D. Oesterhelt, Complementation of a reaction center–deficient *Rhodobacter sphaeroides pufLMX* deletion strain in *trans* with *pufBALM* does not restore the photosynthesis-positive phenotype, J. Bacteriol. 172 (1990) 977–985.
[28] T.G. Lilburn, C.E. Haith, R.C. Prince, J.T. Beatty, Pleiotropic effects of *Pufx* gene deletion on the structure and function of the photosynthetic apparatus of *Rhodobacter capsulatus*, Biochim. Biophys. Acta 1100 (1992) 160–170.
[29] P. McGlynn, C.N. Hunter, M.R. Jones, The *Rhodobacter sphaeroides* PufX protein is not required for photosynthetic competence in the absence of a light harvesting system, FEBS Lett. 349 (1994) 349–353.
[30] F. Francia, J. Wang, H. Zischka, G. Venturoli, D. Oesterhelt, Role of the N- and C-terminal regions of the PufX protein in the structural organization of the photosynthetic core complex of *Rhodobacter sphaeroides*, Eur. J. Biochem. 269 (2002) 1877–1885.
[31] C.A. Siebert, P. Qian, D. Fotiadis, A. Engel, C.N. Hunter, P.A. Bullough, Molecular architecture of photosynthetic membranes in *Rhodobacter sphaeroides*: the role of PufX, EMBO J. 23 (2004) 690–700.
[32] E.C. Ratcliffe, R.B. Tunnicliffe, I.W. Ng, P.G. Adams, P. Qian, K. Holden-Dye, M.R. Jones, M.P. Williamson, C.N. Hunter, Experimental evidence that the membrane-spanning helix of PufX adopts a bent conformation that facilitates dimerisation of the *Rhodobacter sphaeroides* RC–LH1 complex through N-terminal interactions, Biochim. Biophys. Acta, Bioenerg 1807 (2011) 95–107.
[33] R.A. Niederman, D.E. Mallon, J.J. Langan, Membranes of *Rhodopseudomonas sphaeroides*. IV. Assembly of chromatophores in low-aeration cell suspensions, Biochim. Biophys. Acta 440 (1976) 429–447.
[34] J. Takemoto, Kinetics of photosynthetic membrane protein assembly in *Rhodopseudomonas spheroides*, Arch. Biochem. Biophys. 163 (1974) 515–520.
[35] C.N. Hunter, N.G. Holmes, O.T.G. Jones, R.A. Niederman, Membranes of *Rhodopseudomonas sphaeroides*. VII. Photochemical properties of a fraction enriched in newly synthesized bacteriochlorophyll α-protein complexes, Biochim. Biophys. Acta 548 (1979) 253–266.
[36] C.N. Hunter, J.D. Pennoyer, J.N. Sturgis, D. Farrelly, R.A. Niederman, Oligomerization states and associations of light-harvesting pigment protein complexes of *Rhodobacter sphaeroides* as analyzed by lithium dodecyl-sulfate polyacrylamide-gel electrophoresis, Biochemistry 27 (1988) 3459–3467.
[37] J.D. Olsen, J.D. Tucker, J.A. Timney, P. Qian, C. Vassilev, C.N. Hunter, The organization of LH2 complexes in membranes from *Rhodobacter sphaeroides*, J. Biol. Chem. 283 (2008) 30772–30779.
[38] R.N. Frese, J.C. Pàmies, J.D. Olsen, S. Bahatyrova, C.D. van der Weij-de Wit, T.J. Aartsma, C. Otto, C.N. Hunter, D. Frenkel, R. van Grondelle, Protein shape and crowding drive domain formation and curvature in biological membranes, Biophys. J. 94 (2008) 640–647.
[39] P. McGlynn, C.N. Hunter, M.R. Jones, The *Rhodobacter sphaeroides* PufX protein is not required for photosynthetic competence in the absence of a light harvesting system, FEBS Lett. 349 (1994) 349–353.
[40] P. McGlynn, W.H.J. Westerhuis, M.R. Jones, C.N. Hunter, Consequences for the organization of reaction center–light harvesting antenna 1 (LH1) core complexes of *Rhodobacter sphaeroides* arising from deletion of amino acid residues from the C terminus of the LH1 α polypeptide, J. Biol. Chem. 271 (1996) 3285–3292.
[41] C.N. Hunter, P. McGlynn, M.K. Ashby, J.G. Burgess, J.D. Olsen, DNA sequencing and complementation/deletion analysis of the *bchA-puf* operon region of *Rhodobacter sphaeroides*: *in vivo* mapping of the oxygen-regulated *puf* promoter, Mol. Microbiol. 5 (1991) 2649–2661.
[42] X. Zeng, M. Choudhary, S. Kaplan, A second and unusual *pucBA* operon of *Rhodobacter sphaeroides* 2.4.1: genetics and function of the encoded polypeptides, J. Bacteriol. 185 (2003) 6171–6184.
[43] X.M. Song, W. Connor, K. Hokamp, L.A. Babiuk, A.A. Potter, The growth phase-dependent regulation of the pilus locus genes by two-component system TCS08 in *Streptococcus pneumoniae*, Microb. Pathog. 46 (2009) 28–35.
[44] N. Desroche, C. Beltramo, J. Guzzo, Determination of an internal control to apply reverse transcription quantitative PCR to study stress response in the lactic acid bacterium *Oenococcus oeni*, J. Microbiol. Methods 60 (2005) 325–333.
[45] B.M. Hopkinson, K.L. Roe, K.A. Barbeau, Heme uptake by *Microscilla marina* and evidence for heme uptake systems in the genomes of diverse marine bacteria, Appl. Environ. Microbiol. 74 (2008) 6263–6270.
[46] H. Sztajer, A. Lemme, R. Vilchez, S. Schulz, R. Geffers, C.Y. Yip, C.M. Levesque, D.G. Cvitkovitch, I. Wagner-Dobler, Autoinducer-2-regulated genes in *Streptococcus mutans* UA159 and global metabolic effect of the *luxS* mutation, J. Bacteriol. 190 (2008) 401–415.
[47] R.K. Clayton, Spectroscopic analysis of bacteriochlorophylls *in vitro* and *in vivo*, Photochem. Photobiol. 5 (1966) 669–677.
[48] P.A. Reilly, R.A. Niederman, Role of apparent membrane growth initiation sites during photosynthetic membrane development in synchronously dividing *Rhodopseudomonas sphaeroides*, J. Bacteriol. 167 (1986) 153–159.
[49] J.N. Sturgis, R.A. Niederman, The effect of different levels of the B800–850 light-harvesting complex on intracytoplasmic membrane development in *Rhodobacter sphaeroides*, Arch. Microbiol. 165 (1996) 235–242.
[50] S. Scheuring, J. Seguin, S. Marco, D. Levy, B. Robert, J.L. Rigaud, Nanodissection and high-resolution imaging of the *Rhodopseudomonas viridis* photosynthetic core complex in native membranes by AFM, Proc. Natl. Acad. Sci. USA 100 (2003) 1690–1693.
[51] D. Fotiadis, P. Qian, A. Pilippsen, P.A. Bullough, A. Engel, C.N. Hunter, Structural analysis of the RC–LH1 photosynthetic core complex of *Rhodospirillum rubrum* using atomic force microscopy, J. Biol. Chem. 279 (2004) 2063–2068.
[52] S. Scheuring, R.P. Goncalves, V. Prima, J.N. Sturgis, The photosynthetic apparatus of *Rhodopseudomonas palustris*: structures and organization, J. Mol. Biol. 358 (2006) 83–96.
[53] M.Z. Papiz, S.M. Prince, T. Howard, R.J. Cogdell, N.W. Isaacs, The structure and thermal motion of the B800–850 LH2 complex from *Rps. acidophila* at 2.0 Å over-circle resolution and 100 K: new structural features and functionally relevant motions, J. Mol. Biol. 326 (2003) 1523–1538.
[54] S. Scheuring, J. Seguin, S. Marco, D. Levy, C. Breyton, B. Robert, J.L. Rigaud, AFM characterization of tilt and intrinsic flexibility of *Rhodobacter sphaeroides* light harvesting complex 2 (LH2), J. Mol. Biol. 325 (2003) 569–580.
[55] G.S. Inamine, J. van Houten, R.A. Niederman, Intracellular localization of photosynthetic membrane growth initiation sites in *Rhodopseudomonas sphaeroides*, J. Bacteriol. 158 (1984) 425–429.
[56] S.J. Jamieson, P. Wang, P. Qian, J.Y. Kirkland, M.J. Conroy, C.N. Hunter, P.A. Bullough, Projection structure of the photosynthetic reaction centre-antenna complex of *Rhodospirillum rubrum* at 8.5 Å resolution, EMBO J. 21 (2002) 3927–3935.
[57] A.W. Roszak, T.D. Howard, J. Southall, A.T. Gardiner, C.J. Law, N.W. Isaacs, R.J. Cogdell, Crystal structure of the RC–LH1 core complex from *Rhodopseudomonas palustris*, Science 302 (2003) 1969–1972.